Mecánica Computacional Vol. XXIII, pp. 2031-2045
G.Buscaglia, E.Dari, O.Zamonsky (Eds.)
Bariloche, Argentina, November 2004

DIRECT NUMERICAL SIMULATIONS OF AXISYMMETRIC DENSITY CURRENTS

Mariano I. Cantero*, James P. Ferry†, S. Balachandar‡, and Marcelo H. García*

*Department of Civil and Environmental Engineering
University of Illinois at Urbana-Champaign
205 N. Mathews Avenue, Urbana, Illinois 61801, USA
e-mail: mcantero/mhgarcia@uiuc.edu, web page: http://www.vtchl.uiuc.edu

†Center for the Simulation of Advanced Rockets
University of Illinois at Urbana-Champaign
1304 W. Springfield Avenue, Urbana, Illinois 61801, USA
e-mail: jpferry@uiuc.edu, web page: http://www.csar.uiuc.edu

‡Department of Theoretical and Applied Mechanics
University of Illinois at Urbana-Champaign
104 S. Wright Street, Urbana, Illinois 61801, USA
e-mail: s-bala@uiuc.edu, web page: http://www.tam.uiuc.edu

Key Words: Density Currents, Gravity Currents, Stratified Flow, Kelvin-Helmholtz Instabilities, Direct Numerical Simulation, Spectral Method.

Abstract. *Three dimensional direct numerical simulations are presented for axisymmetric density currents using the Boussinesq approximation for small density difference. Three Gr numbers are investigated (10^5, 1.5×10^6 and 10^7) in order to identify differences in the flow structure and dynamics, and to compare with planar density currents.*

The simulations are performed using a fully de-aliased pseudospectral method. The simulated flows present the main features observed in experiments for the large Gr numbers. The front location and velocity computed show that the Fr relation used to close the box model and shallow water models for density currents must be corrected to account for Gr and geometrical dependencies.

1 INTRODUCTION

When two fluids with different densities interact freely over a rigid bottom they manifest as density currents. Examples of these flows are snow avalanches, thunderstorm fronts, volcano eruptions, oil spills on the ocean, the release of contaminants in the environment and flows generated by the collapse of a building. Many more examples can be found in the books by Simpson[1] and Allen.[2] In most environmental and industrial flows of this type the density difference is of only a few percents and it is caused by chemical constitution, temperature, salinity or particles in suspension.

We consider the release of a cylindrical region of denser fluid in a slightly less dense ambient. The released volume has initial radius r_0 and initial height $2\,h_0$ (see figure 1). Soon after the release a density current develops, which presents a front, a body and a tail. The front is a discontinuity in density that travels over a thin layer of light fluid, as a consequence of the no-slip condition at the bottom. The front of the current is a complex, dynamic region where most of the mixing occurs. This mixing, driven by Kelvin-Helmholtz instabilities and vortex shedding, plays an important role regulating the flow since it modifies the driving force by entraining ambient fluid into the current, and thus, diminishing the negative buoyancy. Behind the front, the body and the tail form, and how long they extend depends on the initial condition. In this region, the vortices shed from the front pair, stretch and break down.

In the past numerous theoretical and experimental works on planar and axisymmetric density currents were conducted. The first theoretical attempts to describe the front velocity were done by von Kármán[3] and Benjamin.[4] Benjamin[4] found that in a lock-exchange configuration the front should move at a dimensionless speed of $1/\sqrt{2}$. Later works used the shallow water theory to describe the dynamics of the front[5–8] and made use of an empirical Froude condition to close the model.

Several experiments have also been performed to study the front dynamics. Huppert and Simpson[9] have studied the release of a fixed volume of denser fluid in a lighter ambient experimentally. They found that initially the current spreads at approximately constant speed and then decelerates, which have been called the slumping and the inertial phases, respectively. They also proposed an empirical Froude condition that has been used in box models and to close shallow water models. Allen[10] and Simpson[11] have devoted great effort to study the lobe and cleft pattern observed at the front in these type of flows, and Parsons and García[12] have studied the similarity of density currents fronts.

Recently, high resolution numerical computations have been performed[13,14] for planar currents. These works have provided a detailed analysis of the flow topology at the foremost part of the current. No such effort has been attempted to date for axisymmetric configurations. We center our attention in the release of a fixed volume of a homogeneous fluid in a slightly less dense environment in axisymmetric configuration and contrast our results to the planar case.

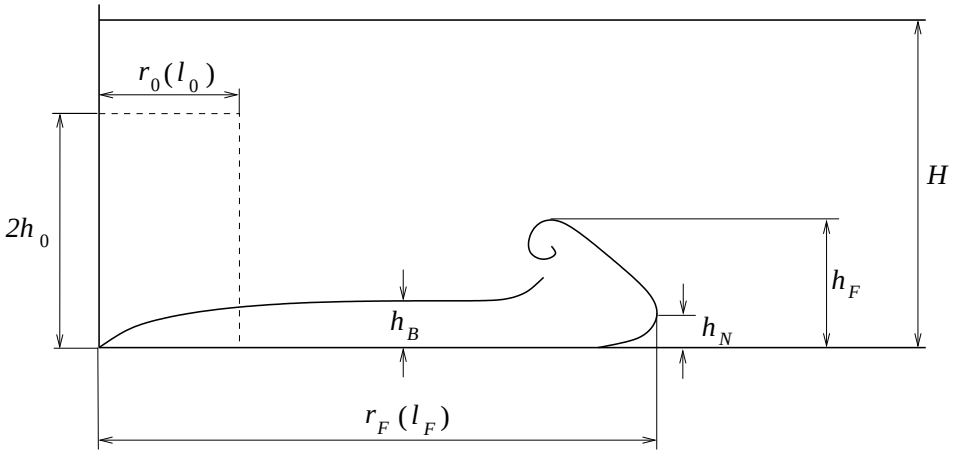

Figure 1: Sketch of a density current showing the main features of the fbw and nomenclature for this work.

2 NUMERICAL FORMULATION

We consider flows in which the density difference is small enough that Boussinesq approximation can be adopted. By this approximation density variations are only incorporated in the buoyancy terms. The dimensionless equations read

$$\frac{\partial \tilde{u}_i}{\partial \tilde{t}} + \tilde{u}_k \frac{\partial \tilde{u}_i}{\partial \tilde{x}_k} = \tilde{\rho}\, e_i - \frac{\partial \tilde{p}}{\partial \tilde{x}_i} + \frac{1}{\sqrt{Gr}} \frac{\partial^2 \tilde{u}_i}{\partial \tilde{x}_k \partial \tilde{x}_k} \tag{1}$$

$$\frac{\partial \tilde{u}_k}{\partial \tilde{x}_k} = 0 \tag{2}$$

$$\frac{\partial \tilde{\rho}}{\partial \tilde{t}} + \frac{\partial}{\partial \tilde{x}_k} (\tilde{\rho} \tilde{u}_k) = \frac{1}{Sc\sqrt{Gr}} \frac{\partial^2 \tilde{\rho}}{\partial \tilde{x}_k \partial \tilde{x}_k}, \tag{3}$$

Here $\tilde{u}_i$ is the velocity vector, $\tilde{p}$ is the dynamic pressure, $\tilde{\rho}$ is the density, Gr is the Grashof number, Sc is the Schmidt number and e_i is a unitary vector pointing in the gravity direction. We have adopted the channel half size, h_0, as the length scale. Since there is no externally-imposed velocity scale for the flow, we have adopted

$$U_0 = \sqrt{g \frac{\rho_1 - \rho_0}{\rho_0} h_0} \tag{4}$$

as the velocity scale. Consequently, the time scale is h_0/U_0. Here ρ_1 is the density of the denser fluid and ρ_0 is the density of the ambient fluid. The dimensionless density and dynamic pressure are given by

$$\tilde{\rho} = \frac{\rho - \rho_0}{\rho_1 - \rho_0}, \qquad \tilde{p} = \frac{p}{\rho_0 U_0^2}. \tag{5}$$

The two dimensionless numbers in equations (1)–(3) are

$$Gr = \left(\frac{U_0\, h_0}{\nu}\right)^2 \qquad \text{and} \tag{6}$$

$$Sc = \frac{\nu}{\kappa}, \tag{7}$$

where ν is the kinematic viscosity and κ is the diffusivity of temperature or salinity responsible for the density difference. The Gr number plays the role of the square of the Reynolds number. We have decided to called it Gr because it uses a velocity scale derived from the buoyancy terms, and to be consistent with the notation used by Härtel *et al.*[13] to allow for comparison of the results. The ratios r_0/h_0 and h_0/H are additional geometric parameters introduced by the initial condition. In this work we will concentrate on the condition $H = 2h_0$.

The governing equations are solved using a de-aliased pseudospectral code.[15] Fourier expansions are employed for the flow variables in the horizontal directions (x and y). In the inhomogeneous vertical direction (z) Chebyshev expansion is used with Gauss-Lobatto quadrature points. The flow field is time advanced using a Crank-Nicholson scheme for diffusion terms. The advection terms are handled with Arakawa's method and advanced with a third-order Runge-Kutta scheme. The buoyancy term is also advanced with a third-order Runge-Kutta scheme. More details on the implementation of this numerical scheme can be found in Cortese and Balachandar.[16]

The computational domain is a box of size $L_x = 20 \times L_y = 20 \times L_z = 2$. Periodic boundary conditions are enforced in the horizontal directions for all variables. At the top and bottom walls no-slip and zero-gradient conditions are enforced for velocity and density, respectively.

3 FLOW STRUCTURE IN THE AXISYMMETRIC CONFIGURATION

We will discuss here the flow structure only for the axisymmetric configuration. The flow structure of the planar case has been discussed in great detail by Härtel *et al.*[13] To study the structure of the flow, simulations for $Gr = 10^5$, 1.5×10^6 and 10^7 were performed. The Sc number was set to 1 since it does not have an influence on the flow as long as it is kept O(1). This observation is consistent with the findings of Härtel *et al.*[13] In these simulations the flow was solved using approximately 6 million grid point for $Gr = 10^5$ and 1.5×10^6, and 10 million grid points for $Gr = 10^7$. The initial condition is a cylindrical region of denser fluid with radius $r_0 = 2$ an height $2h_0 = 2$. A minute random disturbance was prescribed in the density field to accelerate the three-dimensional breakdown. The solution was advanced in time until the front reached the radial location of $r = 8$ to avoid the influence of the lateral boundaries.[17]

Figure 2 shows the time development of the flow structure for the higher Gr number of 10^7. After the release of the denser fluid, an intrusive front forms. Initially, the flow evolves in a two-dimensional fashion (axisymmetric flow) in which Kelvin-Helmholtz rolls develop and form the front and the nose. Below the nose, which is raised from the bottom, an unstable stratified region forms as a consequence of the no-slip condition. In this region, three-dimensional instabilities develop and evolve into a lobe and cleft pattern in the foremost part of the current.

This feature has been observed in experiments for both, planar[11] and axisymmetric currents.[18] Behind the front, the flow develops into a very intense three-dimensional structure where the Kelvin-Helmholtz billows shed from the front deform, bend and break up. This behavior is similar to the planar case.[13,19]

The lobe and cleft structure can be observed in figure 3, where a detailed view of the front is shown. The lobe and cleft evolution can be more clearly observed in figure 4 where we plot on the bottom surface contours of constant density. In contrast to the planar case, the number of lobes in the front does not decrease as the front evolves. It stays rather constant. However, since the current is spreading radially, the size of the lobes grows as the current evolves until the current is dissipated. How this lobe and cleft pattern forms and evolves is highly Gr-dependent. For example, the solution for $Gr = 10^5$ does not present this feature. The solution is completely axisymmetric for all time.

The structure of the mean flow is also dependent on the Gr number. Figure 5 shows density and vorticity contours for $Gr = 10^5$, 1.5×10^6 and 10^7 at $\tilde{t} = 8$. The main features of the current in term of the head and the nose are present for all the Gr numbers investigated. However, they present some differences, mainly in the front shape and nose height. The lower Gr number solution has a more rounded head and a higher nose compared to the higher Gr solution.

4 MEAN FLOW DYNAMICS IN THE AXISYMMETRIC CONFIGURATION

In the following we will describe the dynamics of the mean flow for the axisymmetric configuration. In this configuration the mean values, indicated by an overbar, are computed as

$$\bar{f}(r,z) = \frac{1}{2\pi} \int_0^{2\pi} f(r,\theta,z)\, d\theta. \tag{8}$$

Figure 6 shows mean density contours at $\tilde{t} = 4$, 8 and 10 for $Gr = 10^7$. An impression of how the flow evolves can be gained from this figure. The development of the mean flow starts with a short acceleration phase. In this phase, the nose is formed and the slumping phase velocity is reached. After the initial acceleration phase, the flow enters the slumping phase, in which the current moves at approximately constant speed (which depends on the Gr of the flow). In this phase the flow presents a very interesting dynamics that is shown in figure 7. First, a large billow is formed in the front (B1 in figure 7), which gives the current the characteristic structure of front and body. Then, two more billows are formed. One counter-rotating billow is formed in the lower region of the front (B2), which has been interpreted as a boundary layer separation by Alahyari and Logmire[20] caused by the adverse pressure gradient produced by the first billow (B1). The other billow (B3) is formed in the body of the current and rotates in the same direction as the first billow (B1). Finally, the first billow formed in the front (B1) is retarded with respect to the front, which gives place to the formation of another billow on the upper region of the front (B4). At the same time, billows B2 and B3 loose their identity.

After the slumping phase, the flow enters into a decelerating phase called inertial phase. The box model (presented in the following section) predicts that in the inertial phase the front

location varies as $\tilde{t}^{1/2}$. During this phase the third billow formed at the front (B4) becomes more prominent. This phase will be analyzed in a future work.

5 FRONT VELOCITY

Huppert and Simpson[9] presented the so-called box model to describe the current spreading. This model is based on two assumptions. The first one is about conservation of mass: it is assumed that the current spreads through a serie of equal-volume cylinders of radius r_F and height h_B, *i. e.*

$$(r_0)^2\, 2\, h_0 = (r_F)^2\, h_B \tag{9}$$

The second assumption is about the dynamics of the flow. They postulated that the flow is controlled by the head of the current,[21] and specified a relation between the front velocity (u_F) an the current height just behind the head (Froude condition). Based on experimental measurements they proposed the following empirical relation

$$\frac{u_F}{\sqrt{g\frac{\rho_1-\rho_0}{\rho_0}h_B}} = \begin{cases} \beta\,(h_B/H)^{-\chi} & \text{if } \gamma \leq \frac{h_B}{H} \leq 1 \\ Fr_I & \text{if } 0 \leq \frac{h_B}{H} \leq \gamma \end{cases} \tag{10}$$

for both, axisymmetric and planar currents. The top relation in equation (10) is valid for the slumping phase and the bottom one for the inertial phase. Notice that only three out of the four parameters in equation (10) are independent since $Fr_I = \beta\,\gamma^{-\chi}$. Huppert and Simpson[9] propossed a set of parameters independent of the Gr number and the geometrical configuration: $\beta = 0.5$, $\chi = 0.33$, $\gamma = 0.075$ and $Fr_I = 1.19$. The Froude condition (10) with the set of parameters proposed by Huppert and Simpson[9] have been adopted by many researchers as a key closure relation in their shallow water models.[5–8]

An expression for the front location of the current with time can be derived using the box model. Recalling that

$$u_F = \frac{dr_F}{dt}, \tag{11}$$

and using equations (9) and (10), the following expression can be obtained for the slumping phase of the current

$$(\hat{r}_F)^{1-2\chi}\,\frac{d\hat{r}_F}{d\hat{t}} = \sqrt{2}\,\beta\,\left(\frac{2\,h_0}{H}\right)^{-\chi} \tag{12}$$

where

$$\hat{r}_F = \frac{r_F}{r_0} \quad \text{and} \tag{13}$$

$$\hat{t} = \frac{t\,U_0}{r_0}. \tag{14}$$

Equation 12 may be integrated with the condition $\hat{r}_F(\hat{t}=0)=1$ to obtain

$$\hat{r}_F = \left[1+\sqrt{2}\beta\,\left(\frac{2\,h_0}{H}\right)^{-\chi} 2(1-\chi)\,\hat{t}\right]^{\frac{1}{2(1-\chi)}}. \tag{15}$$

Notice that since $\hat{r}_F$ must grow with time it is required that $\chi \leq 1$. The front velocity is derived from (15) and it is given by

$$\hat{u}_F = \sqrt{2}\beta\left(\frac{2\,h_0}{H}\right)^{-\chi}\left[1+\sqrt{2}\beta\,\left(\frac{2\,h_0}{H}\right)^{-\chi} 2(1-\chi)\,\hat{t}\right]^{\frac{2\chi-1}{2(1-\chi)}} \tag{16}$$

Equations (15) and (16) show that the length scale and time scale for the radial spreading of the current in slumping phase are r_0 and r_0/U_0, respectively. This gives the same velocity scale used to make the conservation equation dimensionless, *i. e.* $\tilde{u}_F = \hat{u}_F$.

For small times, equations (15) and (16) may be approximated as

$$(\hat{r}_F)_{AS} \;\simeq\; 1+\sqrt{2}\,\beta\,\left(\frac{2\,h_0}{H}\right)^{-\chi}\hat{t}, \tag{17}$$

$$(\hat{u}_F)_{AS} \;\simeq\; \sqrt{2}\,\beta\,\left(\frac{2\,h_0}{H}\right)^{-\chi}. \tag{18}$$

by performing a Taylor's series approximation around $\hat{t}=0$ and retaining the first order term. Equation (18) indicates that during the slumping phase, at least for the initial time, the current moves at constant speed.

For the inertial phase, in the same way as before, we find that

$$\hat{r}_F \;=\; \left[\hat{r}_{FI}+2\sqrt{2}\,Fr_I\,(\hat{t}-\hat{t}_I)\right]^{1/2} \tag{19}$$

where $\hat{t}_I$ is the time at which the inertial phase starts and $\hat{r}_{FI}$ is the radius of the current at this time. An expression for $\hat{r}_{FI}$ can be obtained from equation (9):

$$\hat{r}_{FI} = \gamma^{-1/2}\,\left(\frac{2\,h_0}{H}\right)^{1/2}, \tag{20}$$

and equation (19) becomes

$$\hat{r}_F \;=\; \gamma^{-1/2}\,\left(\frac{2\,h_0}{H}\right)^{1/2}\left[1+2\sqrt{2}\,Fr_I\,\gamma\,\left(\frac{2\,h_0}{H}\right)^{-1}(\hat{t}-\hat{t}_I)\right]^{1/2}. \tag{21}$$

Then, the current front velocity in the inertial phase is

$$\hat{u}_F \;=\; 2\sqrt{2\gamma}\,Fr_I\,\left(\frac{2\,h_0}{H}\right)^{-1/2}\left[1+2\sqrt{2}\,Fr_I\,\left(\frac{2\,h_0}{H}\right)^{-1}\gamma\,(\hat{t}-\hat{t}_I)\right]^{-1/2}. \tag{22}$$

Equations (21) and (22) can be approximated for $\hat{t} \gg \hat{t}_I$ as

$$(\hat{r}_F)_{AI} \simeq \left(2\sqrt{2}Fr_I\right)^{1/2} \hat{t}^{1/2} \tag{23}$$

$$(\hat{u}_F)_{AI} \simeq \left(\frac{\sqrt{2}}{2}Fr_I\right)^{1/2} \hat{t}^{-1/2} \tag{24}$$

assuming that the second term in the brackets in equations (21) and (22) is larger than one.[9]

Figure 8 shows the front location of the axisymmetric current during the slumping phase for $Gr = 10^5$, 1.5×10^6 and 10^7. The front moves at approximately constant speed. However, it is clear from this figure that the front velocity is dependent on Gr number. This figure also shows the box model prediction for the slumping phase, which agrees well with the numerical solution when the Gr-dependency is accounted for. The front velocity depends also on geometrical configuration. Figure 9 shows the front velocity in the slumping phase for planar and axisymmetric configurations. These results show that the original assumption of a universal set of parameter for the Froude relation (10) have to be modified to account for Gr and geometrical dependencies.

6 CONCLUSIONS

We have presented and discussed the results of three-dimensional direct numerical simulations of axisymmetric density currents. These highly resolved simulations allowed for a detailed analysis and visualization of the flow structure and dynamics. The simulations were performed for $Gr = 10^5$, 1.5×10^6 and 10^7. The large Gr number simulation exhibits the main features observed in experiments.[11,18] The dynamics of the flow computed in the simulations is in ageement with the large Gr experimental observations.[20]

The box model originally presented by Huppert and Simpson[9] predicts well the front location and velocity trends. However, the original values of the parameters presented by those authors for the Froude condition must be corrected to account Gr and geometrical dependencies. These results are also relevant for shallow water models of density currents where the Froude condition is used to close the models.

7 ACKNOWLEDGEMENTS

We gratefully acknowledge the support of the Coastal Geophysics Program of the Office of Naval Research, the Chicago District of the US Army Corps of Engineers, and the Metropolitan Water Reclamation District of Greater Chicago. Support from the National Center for Supercomputer Applications at UIUC is also acknowledged. Mariano Cantero was supported by a Graduate Student Fellowship from the Computational Science and Engineering Program at UIUC. Computer time was provided by Dr. Fady Najjar.

REFERENCES

[1] J. Simpson. *Gravity Currents*. Cambridge University Press, second edition, (1999).

[2] J. Allen. *Principles of Physical Sedimentology*. George Allen and Unwin Ltd, (1985).

[3] T. von Kármán. The engineer grapples with nonlinear problems. *Bull. Am. Math. Soc.*, (1940).

[4] T. Benjamin. Gravity currents and related phenomena. *Journal of Fluid Mechanics*, **31**, 209–248 (1968).

[5] J. Rottman and J. Simpson. Gravity currents produced by instantaneous releases of a heavy fluid in a rectangular channel. *Journal of Fluid Mechanics*, **135**, 95–110 (1983).

[6] R. Bonnecaze, H. Huppert, and J. Lister. Particle-driven gravity currents. *Journal of Fluid Mechanics*, **250**, 339–369 (1993).

[7] M. Hallworth, H. Huppert, J. Phillips, and R. Sparks. Entrainment into two-dimensional and axisymmetric turbulent gravity currents. *Journal of Fluid Mechanics*, **308**, 289–311 (1996).

[8] M. Hallworth, H. Huppert, and M. Ungarish. Axisymmetric gravity currents in a rotating system: experimental and numerical investigations. *Journal of Fluid Mechanics*, **447**, 1–29 (2001).

[9] H. Huppert and J. Simpson. The slumping of gravity currents. *Journal of Fluid Mechanics*, **99**, 785–799 (1980).

[10] J. Allen. Mixing at turbidity current heads, and its geological implications. *Journal of Sedimentary Petrology*, **41**(1), 97–113 (1971).

[11] J. Simpson. Effects of the lower boundary on the head of a gravity current. *Journal of Fluid Mechanics*, **53**(4), 759–768 (1972).

[12] J. Parsons and M. García. Similarity of gravity current fronts. *Physics of Fluids*, **10**(12), 3209–3213 (1998).

[13] C. Härtel, E. Meiburg, and F. Necker. Analysis and direct numerical simulation of the flow at a gravity-current head. Part 1. Flow topology and front speed for slip and no-slip boundaries. *Journal of Fluid Mechanics*, **198**, 189–212 (2000).

[14] F. Necker, C. Härtel, L. Kleiser, and E. Meiburg. High-resolution simulations of particle-driven gravity currents. *International Journal of Multiphase Flow*, **28**, 279–300 (2002).

[15] C. Canuto, M. Hussaini, A. Quarteroni, and T. Zang. *Spectral Methods in Fluid Dynamics*. Springer-Verlag, (1988).

[16] T. Cortese and S. Balachandar. High performance spectral simulation of turbulent flows in massively parallel machines with distributed memory. *International Journal of Supercomputer Applications*, **9**(3), 187–204 (1995).

[17] C. Härtel, L. Kleiser M. Michaud, and C.Stein. A direct numerical simulation approach to the study of intrusion fronts. *Journal of Engineering Mathematics*, **32**, 103–120 (1997).

[18] T. Spicer and J. Havens. Gravity flow and entrainment by dense gases released instantaneously into calm air. In E. List and G. Jirka, editors, *Proceedings of the Third International Symposium on Stratified Flows*, pages 642–651, (1987).

[19] M. Cantero, M. García, G. Buscaglia, F. Bombardelli, and E. Dari. Multidimensional CFD simulation of a discontinuous density current. Thessaloniki, Greece, (2003). XXX IAHR International Congress.

[20] A. Alahyari and E. Longmire. Development and structure of a gravity current head. *Experiments in Fluids*, **20**, 410–416 (1996).

[21] T. Fanellop and G. Waldman. The dynamics of oil slicks – or 'creeping crude. *A.I.A.A. J.*, **41**, 1–10 (1971).

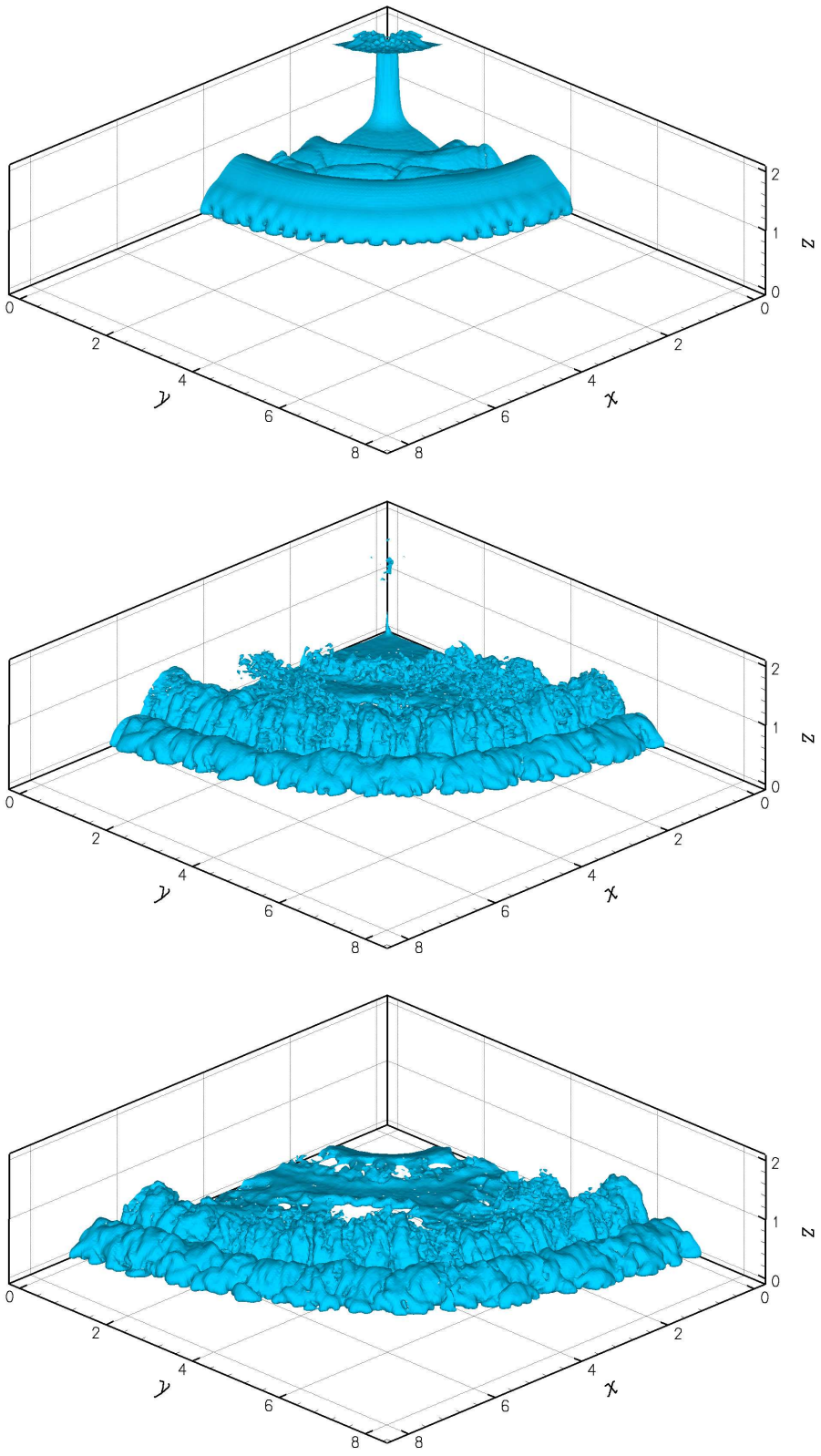

Figure 2: Surface of density 0.3 for $Gr = 10^7$. From top to bottom $\tilde{t} = 4$, 8 and 10. The figure shows only one

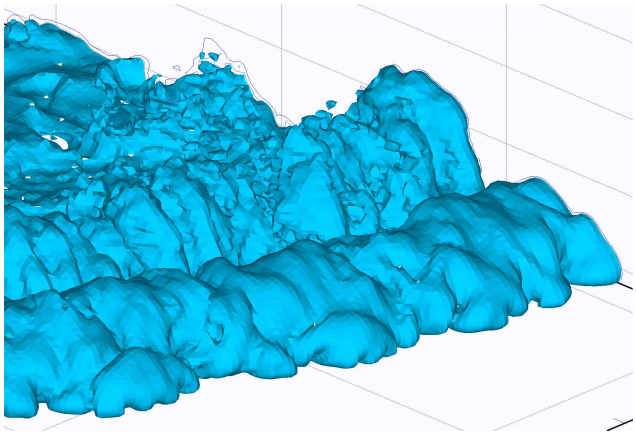

Figure 3: Lobe and cleft pattern for $Gr = 10^7$. Detail of the front at $\tilde{t} = 10$.

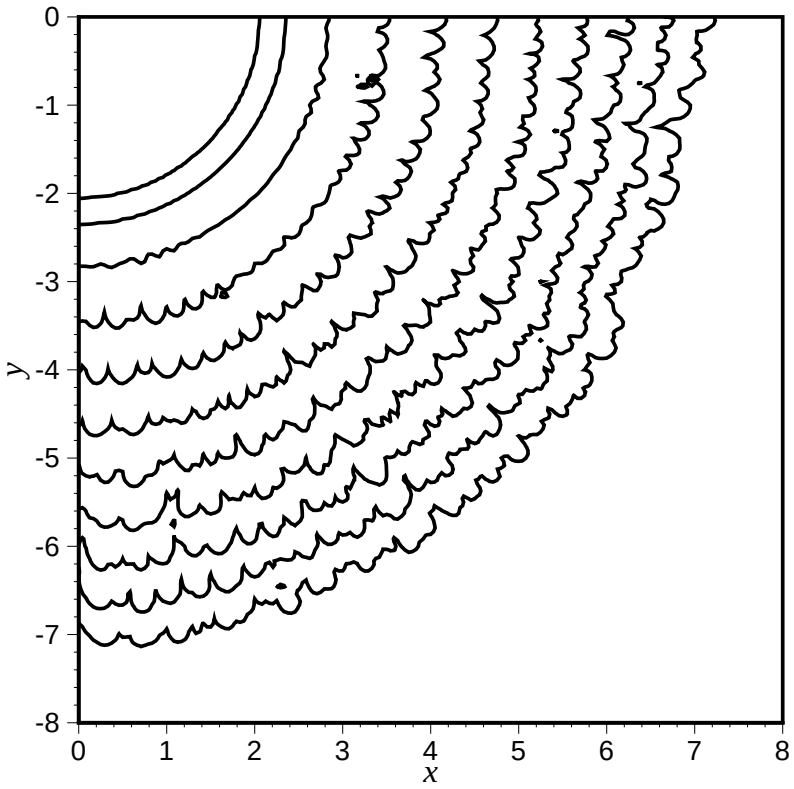

Figure 4: Lobe and cleft pattern for $Gr = 10^7$. Sequence of lobe and clefts visualized by density contours. The fi gure shows only one quadrant of the compuational domain.

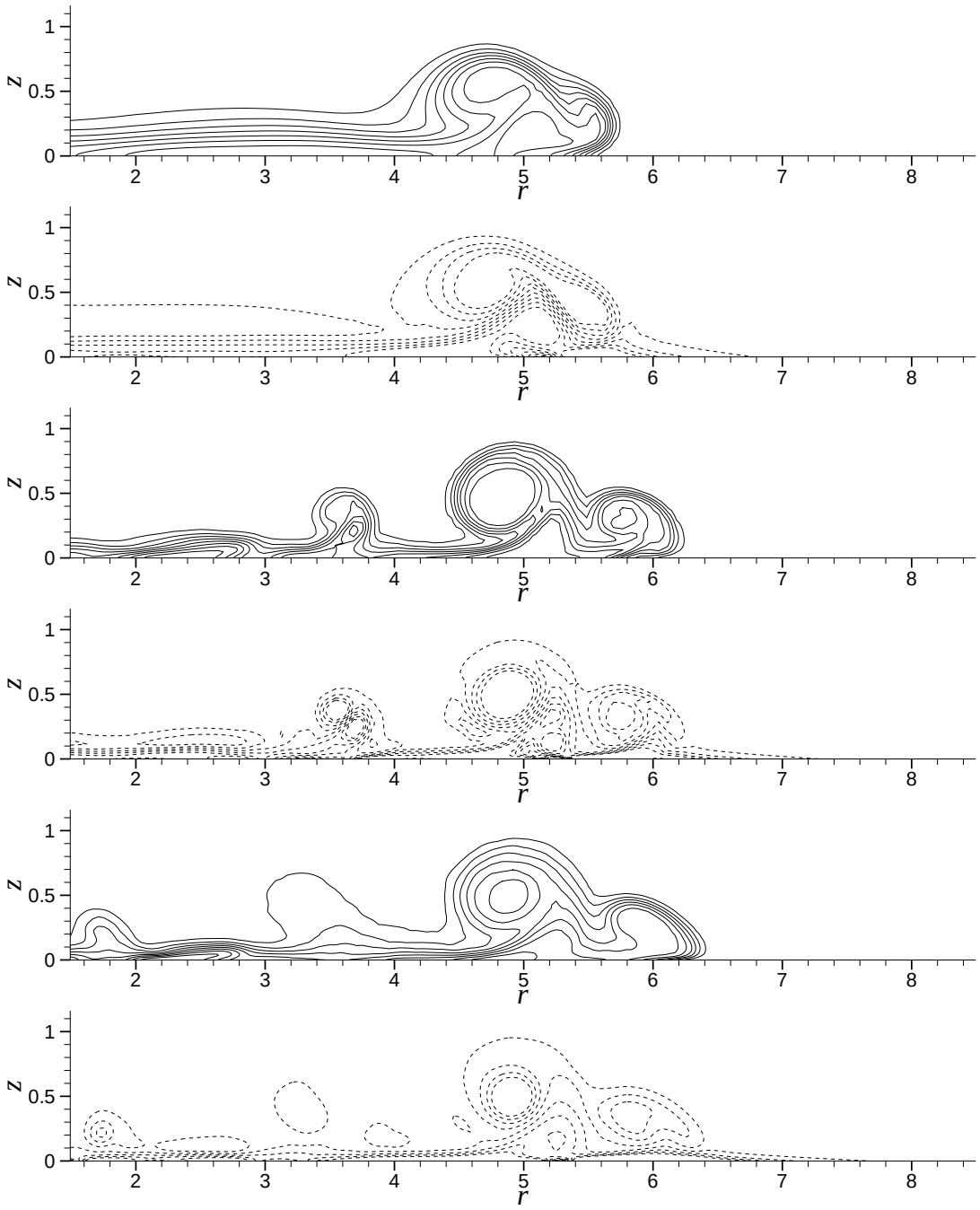

Figure 5: Solid line: mean density contours at $\tilde{t} = 8$. Dashed line: mean vorticity contours at $\tilde{t} = 8$. From top to bottom $Gr = 10^5$, 1.5×10^6 and 10^7.

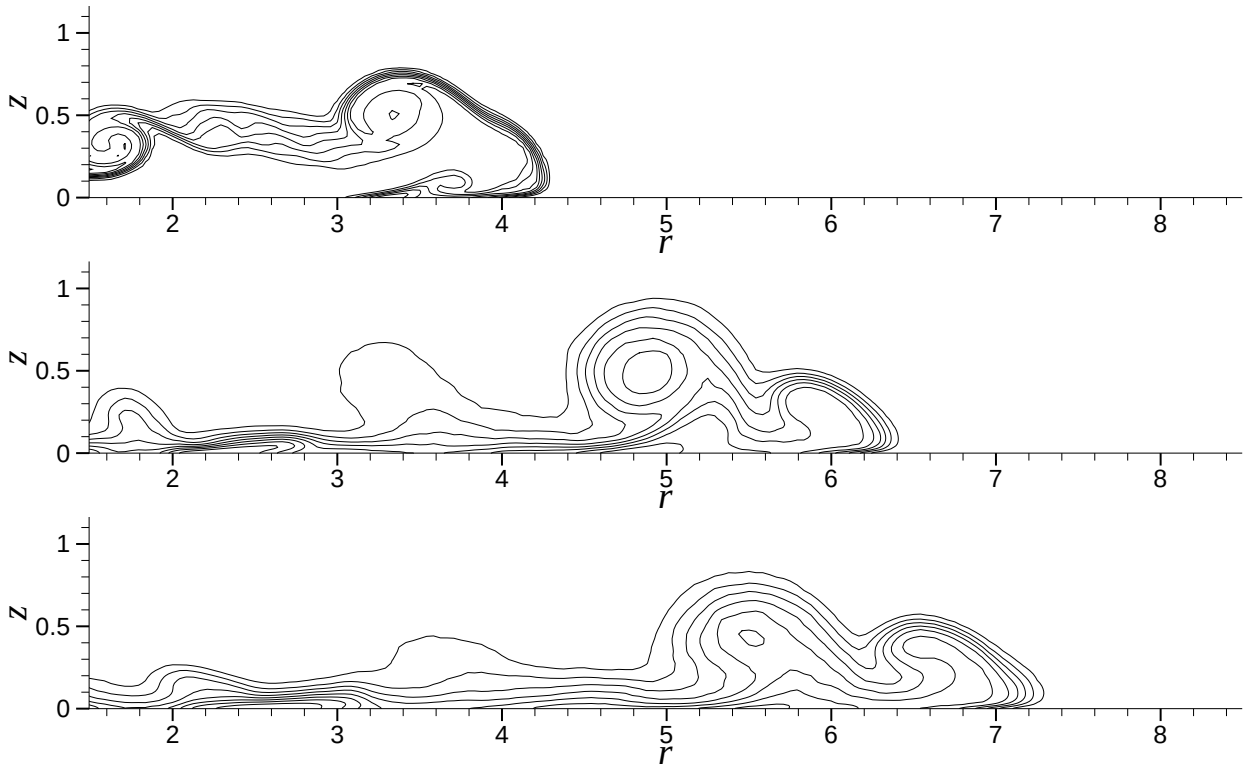

Figure 6: Mean density contours for $Gr = 10^7$. From top to bottom $\tilde{t} = 4$, 8 and 10.

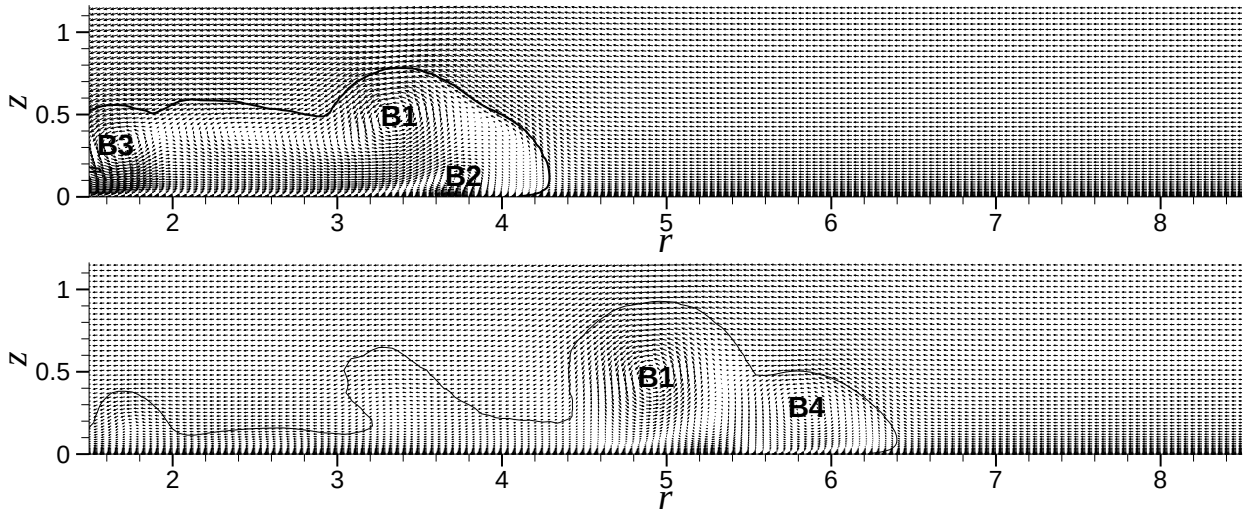

Figure 7: Mean velocity fi eld in the front frame of reference for $Gr = 10^7$. From top to bottom $\tilde{t} = 4$ and 8.

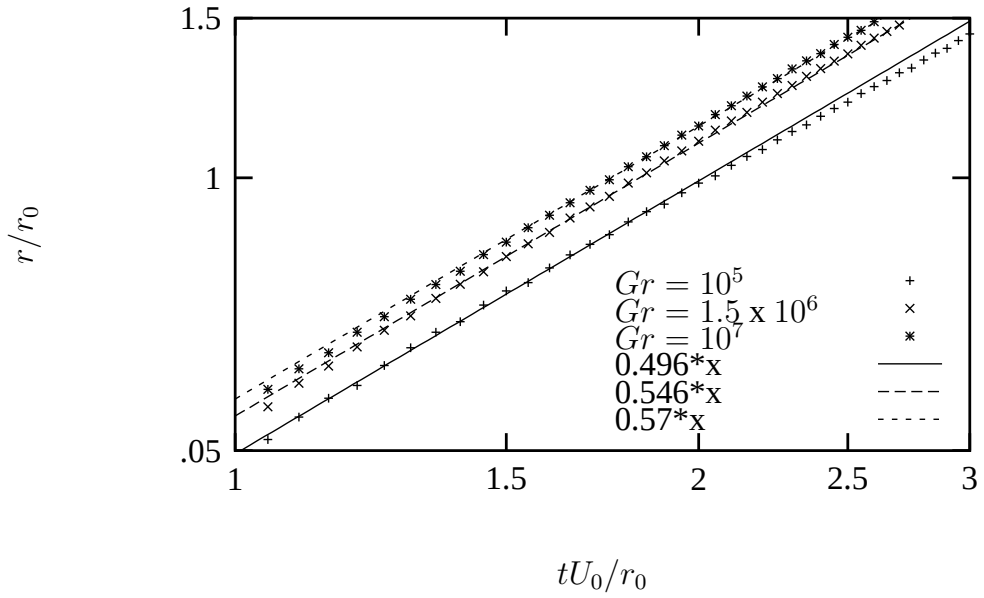

Figure 8: Front location in the slumping phase for axisymmetric current. Log. scales . Simbols: numerical model, lines: box model prediction. The numerical results agree well with the box model prediction when the Gr dependency of the parameters is accounted for.

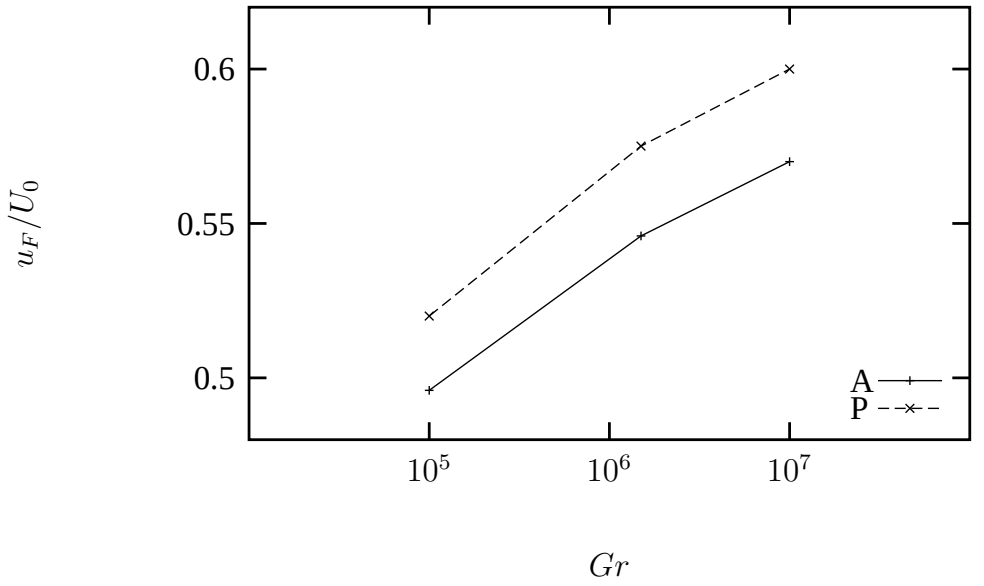

Figure 9: Front velocity in the slumping phase. A: axisymmetric current, P:planar current.